Swell–Shrink–Consolidation Behavior of Rubber–Reinforced Expansive Soils

Amin Soltani [1*], An Deng [2], Abbas Taheri [3] and Asuri Sridharan [4]

[1] PhD Student − School of Civil, Environmental and Mining Engineering, The University of Adelaide, SA 5005, Australia (**Email:** Amin.Soltani@adelaide.edu.au)

[2] Senior Lecturer − School of Civil, Environmental and Mining Engineering, The University of Adelaide, SA 5005, Australia (**Email:** An.Deng@adelaide.edu.au)

[3] Senior Lecturer − School of Civil, Environmental and Mining Engineering, The University of Adelaide, SA 5005, Australia (**Email:** Abbas.Taheri@adelaide.edu.au)

[4] Indian National Science Academy, New Delhi 110002, India; Department of Civil Engineering, Indian Institute of Science, CV Raman Rd, Bangalore 560012, India (retired)

[*] Correspondence: Amin Soltani (**Email:** Amin.Soltani@adelaide.edu.au; **Tel.:** +61–8–83132830; **Fax:** +61–8–83134359)

Abstract: This study examines the effect of two types of recycled tire rubbers of fine and coarse category on the swell–shrink–consolidation behavior of a highly expansive soil mixture. Each of the two rubber choices were incorporated into the soil at four different contents (i.e. rubber to dry soil mass ratio) of 5%, 10%, 20% and 30%. The experimental program consisted of consistency limits, compaction, swell–consolidation, swell–shrink and unconfined compression tests. Improvement in the swell–shrink–consolidation capacity was in favor of higher rubber contents; however, when excessively included raised strength concerns. The swell–shrink–consolidation properties were also rubber size–dependent, meaning that the rubber of coarser size often outperformed the finer rubber. In terms of strength, however, the two rubber types promoted similar results with marginal differences. The results of the unconfined compression tests were cross checked with the swell–shrink–consolidation properties to arrive the optimum stabilization scenarios. A maximum rubber inclusion of 10%, preferably the rubber of coarser category, proved to satisfy the stabilization objectives (i.e. decrease in the swell–shrink–consolidation capacity as well as maintaining or improving the strength), and thus was deemed as the optimum choice. Where context changes and the strength and stiffness is not a primary concern, higher rubber inclusions up to 20% may also be considered acceptable.

Keywords: Expansive soil; recycled tire rubbers; rubber content; rubber size; swell–shrink–consolidation; unconfined compression.

1. Introduction

Expansive soils are low–graded due to their inferior engineering characteristics (e.g. low strength, high compressibility, and a high potential for swelling and shrinkage), and thus are characterized as unsuitable construction materials for the majority engineering applications (Dif and Bluemel 1991; Nalbantoglu 2006; Estabragh et al. 2013a). Where exposed to seasonal environments, such soils are prone to significant volume changes, i.e. heave and settlements, thereby causing instability concerns to the overlying structures. Such concerns have incurred a large amount of maintenance costs, and therefore demands engineering solutions to alleviate the associated socio–economic impacts on human's life (Jones and Jefferson 2012). Stabilization of expansive soils is often achieved through two approaches, i.e. chemical and mechanical techniques (Winterkorn and Pamukcu 1991). Chemical techniques mainly involve the addition of chemical binders, i.e. traditional (e.g. cement, lime and fly–ash) or non–traditional (e.g. polymers, sulfonated oils, resins and enzymes), to the soil mass, thereby amending the soil fabric into a coherent matrix of restricted heave/settlement and induced strength (e.g. Al-Rawas et al. 2005; Mirzababaei et al. 2009; Thyagaraj and Zodinsanga 2014; Onyejekwe and Ghataora 2015; Alazigha et al. 2016; Jha and Sivapullaiah 2016). The mechanical approach makes use of compaction with the aid of reinforcements. Conventional reinforcements include fibers of synthetic (e.g. polypropylene, steel and nylon) or natural (e.g. coir and palm) origin (e.g. Cai et al. 2006; Al-Akhras et al. 2008; Viswanadham et al. 2009a, 2009b; Mirzababaei et al. 2013a; Olgun 2013; Estabragh et al. 2014; Phanikumar and Singla 2016; Shahbazi et al. 2017; Soltani et al. 2017a). As the global community is shifting towards a more sustainable mindset, alternate stabilization techniques capable of replacing or minimizing the use of such conventional agents have been highly encouraged. Beneficial reuse of solid waste materials and industrial by-products may be

regarded amongst the most well-received propositions in this context. The proposition not only addresses the expansive soil problem, but also offers a sound solution to minimizing the environmental impacts associated with waste materials.

Discarded tires have become an ongoing environmental crisis, particularly in industrialized countries where tire stockpiles have reached alarming volumes. In Australia, for instance, it is estimated that 48 million tires are disposed each year, signifying a relative abundance of waste tires available for beneficial reuse (Hannam 2014). Waste tires have excellent mechanical properties (e.g. durability, resiliency and frictional resistance), promoting them as an attractive material for geotechnical applications such as soil stabilization (Zornberg et al. 2004). Similar to fiber–reinforced soils, the rubber assemblage randomly distributes in the soil regime, and where optimized in dosage and geometry, could potentially ameliorate the expansive soil with respect to moisture insensitivity (i.e. swell–shrink related volume changes), compressibility, strength and ductility (e.g. Edil and Bosscher 1994; Cetin et al. 2006; Akbulut et al. 2007; Seda et al. 2007; Özkul and Baykal 2007; Dunham-Friel and Carraro 2011; Patil et al. 2011; Trouzine et al. 2012; Kalkan 2013; Srivastava et al. 2014; Signes et al. 2016; Yadav and Tiwari 2017). As such, the rubber–reinforcement mechanism is expected to be primarily a function of rubber content. However, the rubber's geometrical properties, hereafter referred to as rubber size, could also portray an equally important role in yielding an effective stabilization scheme. The latter should be somewhat similar to the aspect ratio (i.e. fiber length to diameter ratio) in fiber–reinforced soils, which has been well documented in the aforementioned fiber–reinforcement literature. With rubbers, however, this aspect has not yet been adequately addressed in the literature (e.g. Cetin et al. 2006; Srivastava et al. 2014), suggesting further examination into the rubber-reinforcement technique as an ad hoc stabilization solution.

To address the uncertainties associated with selecting effective soil–rubber proportions, this study intends to evaluate the effect of two types of recycled tire rubbers: fine and coarse-grained sizes, on the swell–shrink–consolidation behavior of a highly expansive soil mixture. A series of unconfined compression tests were carried out. The results were cross checked with the swell, shrink and consolidation performance to arrive at the optimum stabilization scenarios.

2. Materials and Methods

2.1. *Expansive Soil*

Commercially available kaolinite and bentonite were used for this study. A mixture of 85% kaolinite and 15% bentonite was selected as the expansive soil for further experimental work. This mixture, hereafter simply referred to as soil, was characterized as *clay with high plasticity* (CH) in accordance with the Unified Soil Classification System (USCS). Mechanical properties of kaolinite, bentonite and the kaolinite–bentonite mixture, determined as per relevant ASTM or Australian standards, are summarized in **Table 1**. Chemical composition of the kaolinite and bentonite, as supplied by the manufacturer, are provided in **Table 2**. The free swell ratio for kaolinite, bentonite and the kaolinite–bentonite mixture was 1.19, 7.53 and 2.91, respectively, from which these soils were graded into *lowly expansive*, *very highly expansive* and *highly expansive*, respectively, in accordance with the classification criteria proposed by Prakash and Sridharan (2004).

Table 1. Mechanical properties of kaolinite, bentonite and the expansive soil mixture.

Properties	Kaolinite	Bentonite	Expansive soil	Standard designation
Specific gravity, G_s	2.68	3.30	2.73	ASTM D854 (2014)
Clay (<2 μm) (%)	49.78	62.43	N/A [1]	ASTM D422 (2007)
Silt (2–75 μm) (%)	49.43	35.75	N/A	ASTM D422 (2007)
Sand (0.075–2 mm) (%)	0.79	1.82	N/A	ASTM D422 (2007)
Liquid limit, *LL* (%)	41.04	379.21	59.60	AS 1289.3.9.1 (2015)
Plastic limit, *PL* (%)	23.67	45.18	27.28	AS 1289.3.2.1 (2009)
Linear shrinkage, LS (%)	N/A	N/A	8.19	AS 1289.3.4.1 (2008)
Plasticity index, *PI* (%)	17.37	334.03	32.32	AS 1289.3.3.1 (2009)
Free swell ratio, *FSR* [2]	1.19	7.53	2.91	Prakash and Sridharan (2004)
USCS classification	CL	CH	CH	ASTM D2487 (2011)
Optimum water content, ω_{opt} (%)	19.82	36.34	26.00	ASTM D698 (2012)
Maximum dry unit weight, γ_{dmax} (kN/m^3)	15.67	11.74	15.07	

[1] not measured; and [2] ratio of equilibrium sediment volume of 10 gr oven–dried soil passing sieve 425 μm in distilled water to that of kerosene.

Table 2. Chemical composition of kaolinite and bentonite (as supplied by the manufacturer).

Properties	Kaolinite	Bentonite
SiO_2 (%)	64.9	63.2
Al_2O_3 (%)	22.2	13.3
TiO_2 (%)	1.4	0.3
Fe_2O_3 (%)	1.0	2.6
CaO (%)	0.1	0.3
Na_2O (%)	0.2	1.9
MgO (%)	0.6	2.2
K_2O (%)	2.7	0.2
Acidity, Ph	7.4	9.5
LOI at 1000 °C (%) [1]	6.5	16.0
CEC (meq/100mL) [2]	N/A [3]	82
SSA (m^2/gr) [4]	11.2	N/A

[1] loss on ignition; [2] cation exchange capacity; [3] not available; and [4] specific surface area.

2.2. *Tire Rubbers*

Two types of commercially available recycled tire rubbers, commonly traded as rubber crumbs and rubber buffings, were used as the reinforcements. Hereafter, these rubber types will be referred to as rubbers A and B, respectively. The grain size distribution curves for kaolinite, bentonite, and rubbers A and B, determined as per the ASTM D422 (2007) standard, are shown in **Figure 1**. Rubber A can be assumed similar in size to fine sand, having an average particle size ranging between 1.18 mm and 75 µm (d_{50}=0.461 mm). Rubber B, however, falls into the coarse sand category, having an average particle size ranging between 4.75 mm and 1.18 mm (d_{50}=1.582 mm). Both rubber types can be classified as poorly-graded sand or SP (in accordance with USCS), in terms of uniformity and curvature coefficients of C_u=2.81 and C_c=1.20 for rubber A, and C_u=1.56 and C_c=1.04 for rubber B. Each of the two rubber choices were incorporated into the soil at four different contents (defined as rubber to dry soil mass ratio), i.e. R_c=5%, 10%, 20% and 30%. Physical and chemical properties, as supplied by the manufacturer, along with a photograph (to scale) of the rubber particles are provided in **Table 3** and **Figure 2**, respectively.

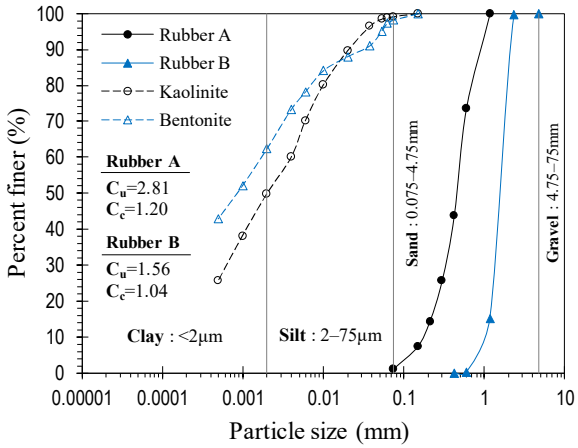

Figure 1. Grain–size distribution curves for kaolinite, bentonite and the tire rubbers.

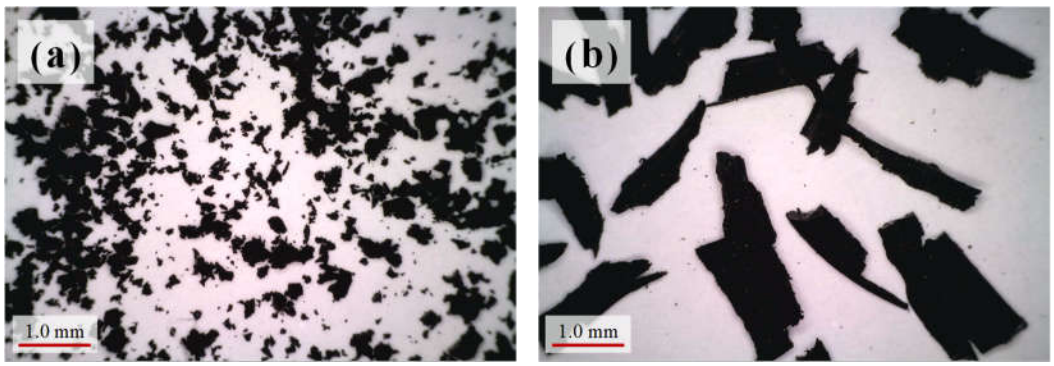

Figure 2. Tire rubbers at 50× magnification: **(a)** rubber A; and **(b)** rubber B.

Table 3. Physical properties and chemical composition of the tire rubbers (as supplied by the manufacturer).

Properties	Value
Physical properties	
Solubility in water	Insoluble
Water adsorption	Negligible
Resistance to acid and alkaline	Excellent
Specific gravity at 20°C	1.09
Particle size for rubber A (mm)	1.18–0.075
Particle size for rubber B (mm)	4.75–1.18
Softening point (°C)	170
Chemical composition	
Styrene–butadiene copolymer (%)	55
Acetone extract (%)	5–20
Carbon black (%)	25–35
Zinc oxide (%)	2.5
Sulphur (%)	1–3

2.3. *Sample Preparation*

A series of standard Proctor compaction tests were carried out on the natural soil and various soil–rubber mixtures in accordance with the ASTM D698 (2012) standard. The results are provided in **Figures 3a** and **3b** for rubbers A and B, respectively. The specific gravity of soil–rubber mixtures, as outlined in **Figure 3**, was estimated by the theoretical relationship proposed by Trouzine et al. (2012). Rubber–reinforcement led to a noticeable decrease in both the optimum water content ω_{opt} and the maximum dry unit weight γ_{dmax} (see the compaction paths in **Figure 3**). The compaction behavior, however, was observed to be independent from the rubber size. Decrease in ω_{opt} and γ_{dmax} can be attributed to the lower specific gravity, larger specific surface area and lower water adsorption of rubber particles compared to soil grains (Özkul and Baykal 2007; Kalkan 2013; Signes et al. 2016).

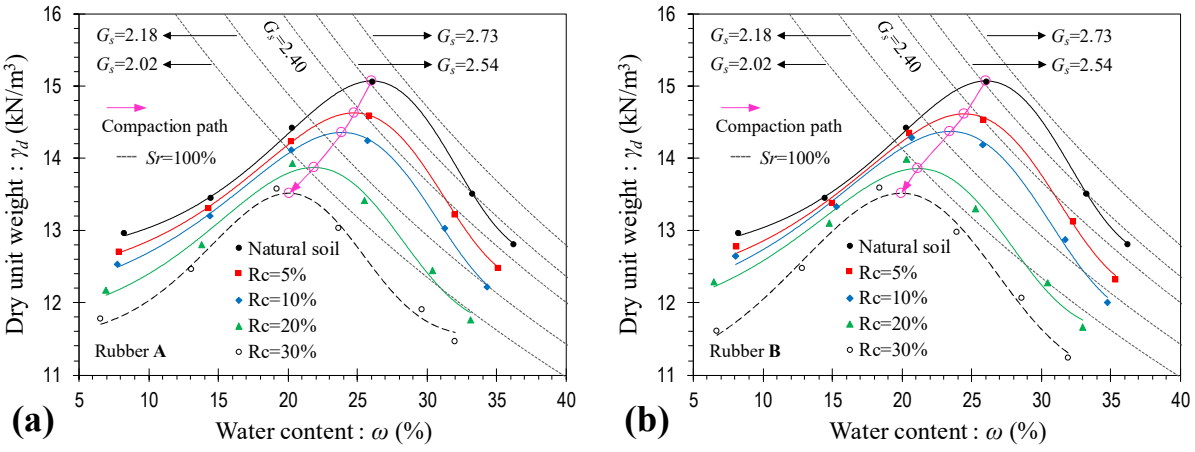

Figure 3. Standard Proctor compaction curves for the natural soil and various soil–rubber mixtures: **(a)** rubber A; and **(b)** rubber B.

Samples for the swell–shrink–consolidation test (see **Section 2.4.1**) were prepared by the static compaction technique at dry of optimum condition (i.e. ω_0=ω_{opt}–5% and its corresponding dry unit weight γ_{d0}). The required amount of water corresponding to the desired water content (see ω_0 in **Table 4**) was added to each mixture, and thoroughly mixed by hand. Extensive care was dedicated to pulverize the lumped particles, targeting homogeneity of mixtures. Mixtures were then enclosed in plastic bags and stored under room temperature conditions for 24 hours, ensuring even distribution of moisture throughout the soil mass. A special split mold, similar to that described in Soltani et al. (2017a), was designed and fabricated from stainless steel to accomplish static compaction. The mold consisted of three sections, i.e. the top collar, the middle oedometer ring and the bottom collar. The oedometer ring measures 50 mm in diameter and 20 mm in height, and accommodates the sample for the swell–shrink–consolidation test. The mixtures were gradually compressed in the mold in three layers to a specific compaction load, each layer having attained the target dry unit weight (see γ_{d0} in **Table 4**). The inner surface of the mold was smeared with a thin layer of

silicon grease to avoid friction during compaction. The surface of the first and second compacted layers were scarified to ensure a good bond between adjacent layers of the mixture. Samples for the unconfined compression (UC) test (see **Section 2.4.2**) were prepared in a similar fashion. In this case, however, a different mold, resulting in samples measuring 50 mm in diameter and 100 mm in height, along with five compaction layers was adopted. In addition, the UC samples were prepared at optimum condition (see ω_{opt} and γ_{dmax} in **Table 4**). Mechanical properties of the prepared samples including the consistency limits and the initial placement conditions are summarized in **Table 4**.

Table 4. Mechanical properties of the prepared samples.

Sample	R_c (%)	LL (%)	PL (%)	PI (%)	ω_{opt} (%)	γ_{dmax} (kN/m^3)	e_{opt} [1]	ω_0 (%)	γ_{d0} (kN/m^3)	e_0 [2]
–	0	59.60	27.28	32.32	26.00	15.07	0.775	21.00	14.52	21.00
Rubber A based sample	5	57.03	27.02	30.01	24.77	14.63	0.706	19.77	14.16	19.77
	10	55.04	25.54	29.50	23.87	14.35	0.639	18.87	13.90	18.87
	20	51.51	23.46	28.05	21.85	13.87	0.541	16.85	13.40	16.85
	30	49.58	22.70	26.88	20.07	13.52	0.469	15.07	12.92	15.07
Rubber B based sample	5	56.88	26.61	30.27	24.47	14.61	0.709	19.47	14.15	19.47
	10	55.62	24.77	30.85	23.46	14.37	0.638	18.46	13.94	18.46
	20	52.44	23.27	29.17	21.15	13.86	0.543	16.15	13.43	16.15
	30	51.21	22.15	29.06	19.94	13.52	0.469	14.94	12.99	14.94

[1] initial placement condition for unconfined compression tests; and [2] initial placement condition for swell–shrink–consolidation tests.

2.4. *Test Procedure*

2.4.1. Swell–Shrink–Consolidation Test

Samples were subjected to a series of swell–shrink–consolidation tests. A typical illustration of the test scheme is provided in **Figure 4**. The swell–consolidation phase, carried out in accordance with the ASTM D4546 (2014) standard, includes two stages, i.e. swell and consolidation. In the first stage, the desired sample is allowed to freely swell under a low nominal overburden stress of σ'_0=1 kPa. The incurred swelling strain was recorded during various time intervals to a point in which swell–time equilibrium, a state corresponding to the sample's swelling potential, could be achieved (see path O→A in **Figure 4a**). During consolidation, the swollen sample, now at state A, is gradually loaded to counteract the built–up swelling strain. The stress required to retain the sample's initial placement or void ratio is taken as the swelling pressure (Sridharan et al. 1986). Upon completion of the loading scheme, the sample is gradually unloaded back to σ'_0=1 kPa (see path A→B_1 for loading, and path B_1→C for unloading in **Figure 4b**). Test results are presented in the form of swelling strain–time (for the swell stage) and void ratio–effective stress (for the consolidation stage) curves plotted over a semi–log space (see **Figures 4a** and **4b**, respectively).

The swell–shrink phase also consists of two stages, i.e. swell and shrink. The swell component is essentially similar to that described in the swell–consolidation test. During the shrink stage, the swollen sample, now at state A, is allowed to desiccate under a constant temperature of 40 °C. The volumetric shrinkage strain along with the corresponding water content were directly measured during various time intervals to a point in which shrinkage ceases (see path A→B_2 in **Figure 4c**). The volumetric shrinkage strain was measured by the volume displacement technique outlined in the ASTM D427 (2004) standard, which has also been commonly adopted in the literature (e.g. Sibley and Williams 1989; Hanafy et al. 1991; Subba Rao et al. 2000; Tripathy et al. 2002; Tripathy and Subba Rao 2009). For the shrink stage, test results are presented in the form of void ratio–water content curves plotted over an arithmetic space (see **Figure 4c**).

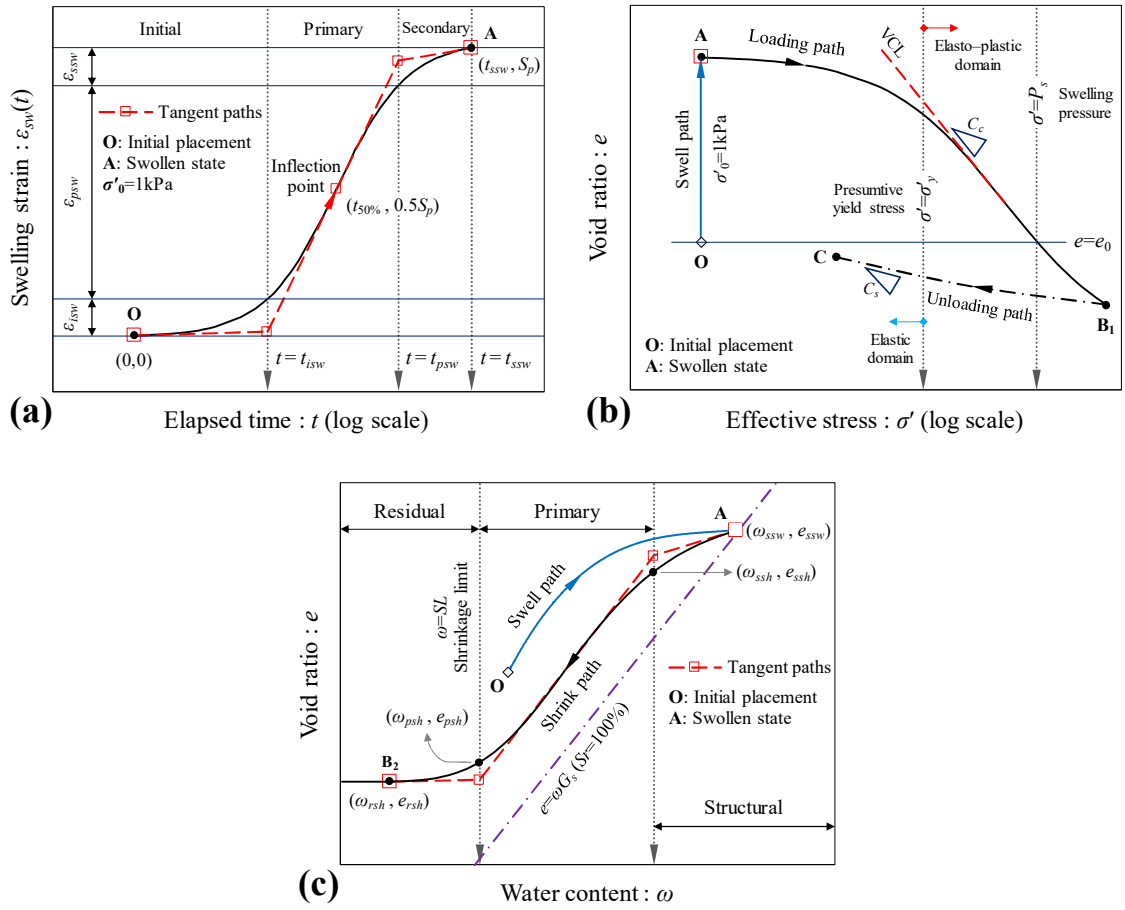

Figure 4. A typical illustration of the swell–shrink–consolidation test scheme: **(a)** swell path; **(b)** consolidation path; and **(c)** shrink path.

2.4.2. Unconfined Compression Test

The unconfined compression test was carried out in accordance with the ASTM D2166 (2016) standard. The samples were compressed by a constant displacement rate of 1 %/min, as commonly adopted in the literature (e.g. Ang and Loehr 2003; Fatahi et al. 2012; Signes et al. 2016). To ensure sufficient accuracy, triplicate samples were tested for each scenario. Axial stress and its corresponding axial strain were recorded during various loading stages to a point of maximum axial stress required for sample failure, denoted as q_u, and its corresponding axial strain, denoted as ε_u, could be achieved. The area under the stress–strain curve up to q_u and ε_u – a measure of the material's ductility defined as energy strain at peak E_p (Maher and Ho 1994; Mirzababaei et al. 2013b) – was also obtained for the tested samples.

3. Results and Discussion

3.1. *Effect of Rubbers on the Swelling Potential*

Swelling strain–time curves, represented by the two–parameter rectangular hyperbola function (e.g. Dakshanamurthy 1978; Sivapullaiah et al. 1996; Sridharan and Gurtug 2004), for the natural soil and various soil–rubber composites are provided in **Figure 5**. As a result of rubber–reinforcement, the swelling strain–time locus experienced a major downward shift over the ε_{sw}:log$t$ space (ε_{sw}=swelling strain; and t=time), indicating a significant reduction in the magnitude of exhibited swelling strain, and thus swelling potential compared to the natural soil. At t=24 hours, for instance, the natural soil displayed a swelling strain of $\varepsilon_{sw}(t)$=15.23%, while the inclusion of 5%, 10%, 20% and 30% rubber A resulted in $\varepsilon_{sw}(t)$=14.99%, 11.82%, 9.01% and 7.67%, respectively (see **Figure 5a**). Similar inclusions of rubber B, however, exhibited a slightly more pronounced decreasing trend where the above given values dropped to $\varepsilon_{sw}(t)$=13.67%, 11.44%, 8.01% and 7.21%, respectively (see **Figure 5b**). The natural soil and soil–rubber A mixtures corresponding to R_c=5%, 10%, 20% and 30% resulted in swelling potential values of S_p=18.35%, 16.02%, 13.01%, 11.17% and 9.56%, respectively. For similar inclusions of rubber B, these values further decreased to S_p=14.74%, 12.18%, 9.02% and 8.11%, respectively.

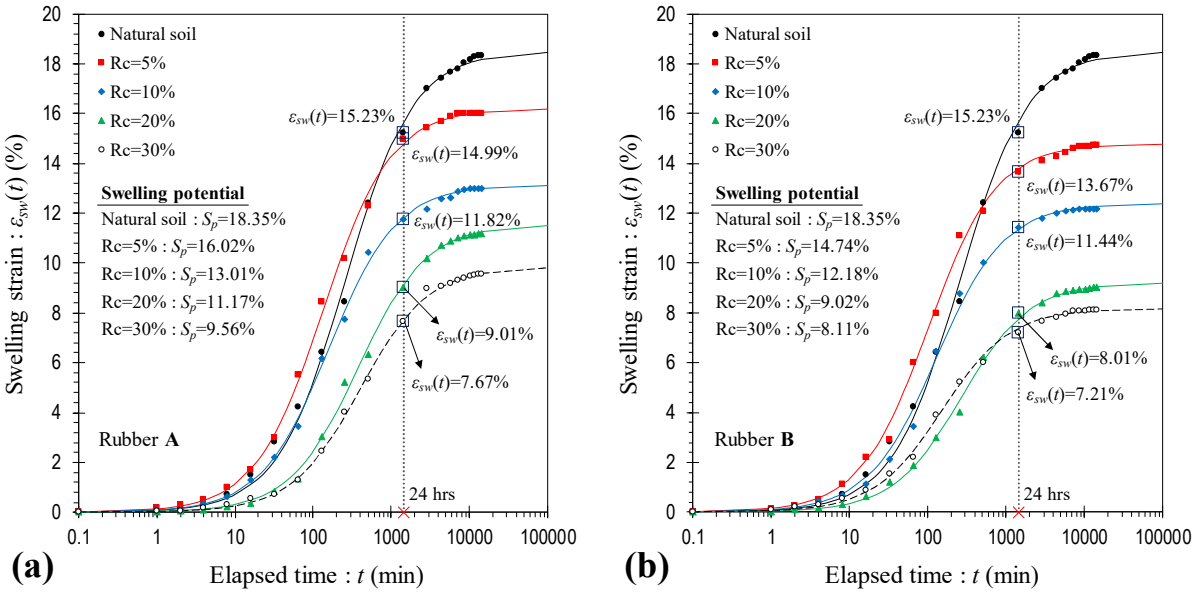

Figure 5. Swelling strain–time curves for the natural soil and various soil–rubber composites: **(a)** rubber A; and **(b)** rubber B.

A typical swell path (see path O→A in **Figure 4a**), plotted over a semi-log space, develops into an *S*-shaped curve, and thus can be divided into three regions, i.e. the initial, primary and secondary swelling, which are defined as phases during which swelling takes place (Dakshanamurthy 1978; Sivapullaiah et al. 1996; Sridharan and Gurtug 2004; Rao et al. 2006; Soltani et al. 2017a). The initial swelling phase, also recognized as inter-void or inter-crystalline swelling, rapidly evolves at macro-structural level, and is accompanied by small volume changes (i.e. $\varepsilon_{isw} \leq 0.1 S_p$). The primary swelling phase constitutes up to 80% of the total volume increase (i.e. $\varepsilon_{psw} \approx 0.8 S_p$), and is graphically bounded by the initial and primary swelling time margins (see **Figure 4a**). The secondary swelling phase occurs as a result of double-layer repulsion, which results in small time-dependent volume changes. In comparison to initial swelling, both the primary and secondary swelling phases evolve at micro-structural level where the swelling of active minerals takes place. Critical variables obtained from the *S*-shaped swell curve are useful concepts capable of describing the time-dependency nature of the swelling phenomenon under field conditions (Sridharan and Gurtug 2004). These variables, defined by a conventional graphical construction as depicted in **Figure 4a**, can be categorized as:

- Completion time of the initial and primary swelling phases, i.e. t_{isw} and t_{psw}.
- Initial, primary and secondary swelling strains, i.e. ε_{isw}, ε_{psw} and ε_{ssw}, where $S_p = \varepsilon_{isw} + \varepsilon_{psw} + \varepsilon_{ssw}$.
- Primary and secondary swelling rates, i.e. C_{psw} and C_{ssw}, which are defined as:

$$C_{psw} = \frac{\Delta \varepsilon_{sw}}{\Delta \log t}\Bigg]_{t_{isw}}^{t_{psw}} = \frac{\varepsilon_{psw}}{\log\left(\frac{t_{psw}}{t_{isw}}\right)} \tag{1}$$

$$C_{ssw} = \frac{\Delta \varepsilon_{sw}}{\Delta \log t}\Bigg]_{t_{psw}}^{t_{ssw}} = \frac{\varepsilon_{ssw}}{\log\left(\frac{t_{ssw}}{t_{psw}}\right)} \tag{2}$$

where t_{ssw}=completion time of the secondary swelling phase (≈240 hours).

Figures 6a and **6b** illustrate the variations of C_{psw} and C_{ssw} against rubber content for the tested samples, respectively. The rubber inclusions led to a noticeable reduction in C_{psw} and C_{ssw}, indicating a capacity to counteract the heave in both magnitude and time. The greater the rubber content the greater the decrease in C_{psw}, following a monotonic trend. Rubber contents greater than 5%, however, did not further deviate C_{ssw}. Rubber B-based samples consistently outperformed rubber A-based samples by exhibiting lower swelling rates for similar rubber inclusions. The natural soil resulted in $C_{psw}=8.38\times10^{-2}$ and $C_{ssw}=2.56\times10^{-2}$. As a typical case, these values, respectively, dropped to 5.89×10^{-2} and 1.54×10^{-2} for rubber A, and 5.58×10^{-2} and 1.19×10^{-2} for rubber B where R_c=10%.

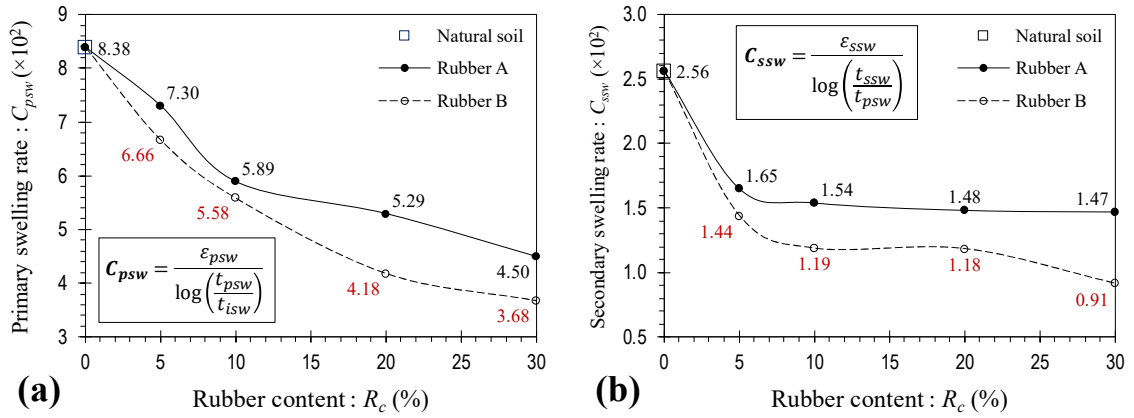

Figure 6. Variations of the **(a)** primary and **(b)** secondary swelling rates against rubber content for the tested samples.

3.2. *Effect of Rubbers on the Consolidation Behavior*

Void ratio–effective stress consolidation curves for the natural soil and various soil–rubber composites are provided in **Figures 7**. A typical consolidation curve with respect to the loading stage (see path A→B_1 in **Figure 4b**), plotted over a semi-log space, develops into a two segment-curvilinear relationship, and thus can be divided into two regions, i.e. the elastic and elasto–plastic compression, which are defined as phases during which consolidation takes place (Sridharan et al. 1991). The two regions are separated by the yield stress, which is commonly interpreted by means of conventional graphical constructions implemented to the e–logσ' or log$e$–logσ' curve (e=void ratio; and σ'=effective stress). Recently, the authors have proposed a subjective–free framework for determination of the yield stress with respect to four common graphical constructions, i.e. the maximum curvature method (Casagrande 1936), the Silva method (Pacheco Silva 1970), the RCL–VCL intercept method (RCL=recompression line; and VCL=virgin compression line), and the log–log method (Jose et al. 1989; Sridharan et al. 1991). Adopting the proposed framework in Soltani et al. (2017b), the average of the four graphical constructions was calculated for each sample, and the results are provided in the form of yield stress paths in **Figure 7**. Rubber–reinforcement led to a slight increase in the yield stress. Natural soil exhibited a yield stress of σ'_y=17.73 kPa. Maximum increase in σ'_y was observed in the case of 30% rubber inclusion, which resulted in σ'_y=23.42 kPa and 22.10 kPa for rubbers A and B, respectively.

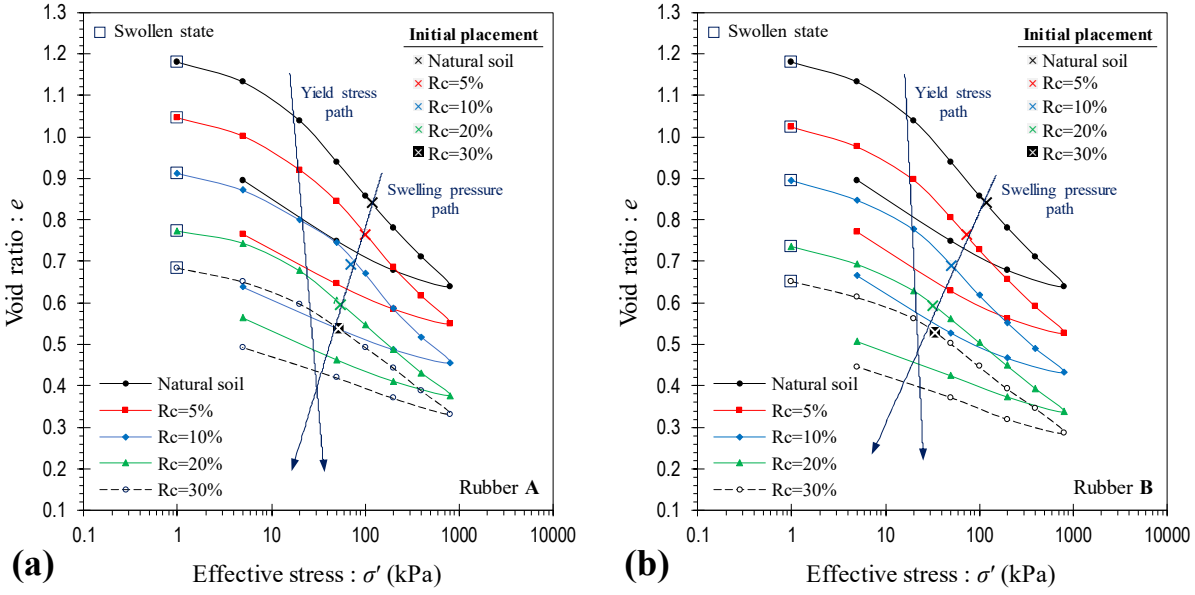

Figure 7. Void ratio–effective stress consolidation curves for the natural soil and various soil–rubber composites: **(a)** rubber A; and **(b)** rubber B.

Figures 8a and **8b** illustrate the variations of the compression index C_c (=slope of the VCL in **Figure 4b**) and the swell index C_s (=slope of the unloading path 'B_1→C' in **Figure 4b**) against rubber content for the tested samples, respectively. The rubber inclusions led to a noticeable reduction in C_c and C_s, indicating a capacity of counteracting

material collapse when stressed. The greater the rubber content the lower the C_c and C_s values, following a monotonic trend. Rubber B often outperformed rubber A in terms of lower C_c values. Regarding C_s, however, the performance of both rubber types seemed to be on par with each other. The natural soil resulted in C_c=0.249 and C_s=0.136. As a typical case, these values, respectively, dropped to 0.191 and 0.087 for rubber A, and 0.187 and 0.078 for rubber B where R_c=20%.

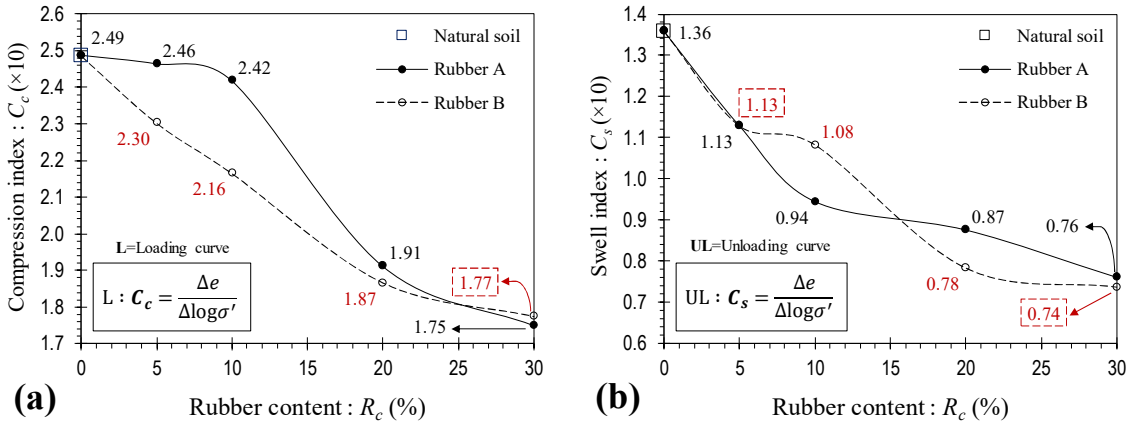

Figure 8. Variations of the **(a)** compression and **(b)** swell indices against rubber content for the tested samples.

Rubber–reinforcement altered the void ratio–effective stress locus, resulting in a major downward shift over the e:logσ' space. As a result, major variations were observed in the swelling pressure (see the swelling pressure paths in **Figure 7**). **Figure 9** illustrates the variations of swelling pressure and swelling potential against rubber content for the tested samples. The variations of swelling pressure P_s followed a trend quite similar to that of swelling potential S_p, indicating that the greater the rubber content the greater the decrease in S_p and P_s. For P_s, however, R_c=30% promoted similar results to R_c=20% with marginal differences, indicating a maximum rubber inclusion of 20% being sufficient to counteract the swelling properties. Similar to S_p, soil–rubber B mixtures consistently outperformed similar samples reinforced with rubber A. The natural soil and soil–rubber mixtures corresponding to R_c=5%, 10%, 20% and 30% resulted in P_s=120.3 kPa, 99.6 kPa, 70.0 kPa, 54.1 kPa, and 51.4 kPa, respectively. With rubber B, these values dropped to P_s=73.0 kPa, 51.0 kPa, 32.2 kPa and 33.6 kPa, respectively.

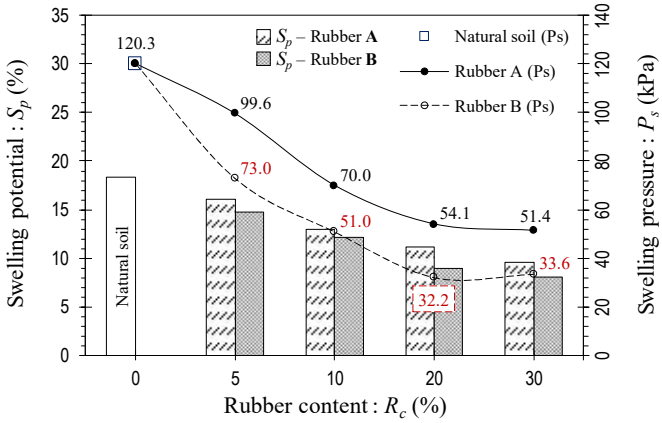

Figure 9. Variations of swelling pressure and swelling potential against rubber content for the tested samples.

The secondary consolidation characteristics were studied under an effective stress of σ'=50 kPa, and the results are provided in **Figure 10**. The completion time of the primary consolidation stage t_{pc} decreased due to the inclusion of rubber A (see **Figure 10a**). This effect, however, was less apparent for samples reinforced with rubber B, which essentially did not deviate t_{pc} (see **Figure 10b**). The secondary consolidation rate C_{sc} can be defined as:

$$C_{sc} = \frac{\Delta \varepsilon_c}{\Delta \log t}\Bigg]_{t_{pc}}^{t_{sc}} = \frac{\varepsilon_{sc}}{\log\left(\frac{t_{sc}}{t_{pc}}\right)} \quad (3)$$

where $\varepsilon_c(t)$=compression strain with respect to elapsed time t; ε_{sc}=secondary consolidation strain; and t_{sc}=completion time of the secondary consolidation stage (=24 hours).

As a result of rubber–reinforcement, the secondary consolidation rate exhibited a noticeable decreasing trend, indicating a capacity to counteract the settlement in both magnitude and time. The natural soil resulted in C_{sc}=7.28×10^{-3}. Where reinforced with 5%, 10%, 20% and 30% rubber A, C_{sc} dropped to 6.05×10^{-3}, 5.57×10^{-3}, 5.34×10^{-3} and 5.02×10^{-3}, respectively. Similar inclusions of rubber B, however, promoted slightly greater values, while still maintaining a noticeable advantage over the natural soil. In this case, R_c=5%, 10%, 20% and 30% resulted in C_{sc}=6.74×10^{-3}, 6.68×10^{-3}, 5.88×10^{-3} and 4.94×10^{-3}, respectively. It is noteworthy to cross check the resulted trends for C_{sc} with C_{ssw}, which are expected to be somewhat consistent and comparable (Sridharan and Gurtug 2004; Phanikumar and Singla 2016).

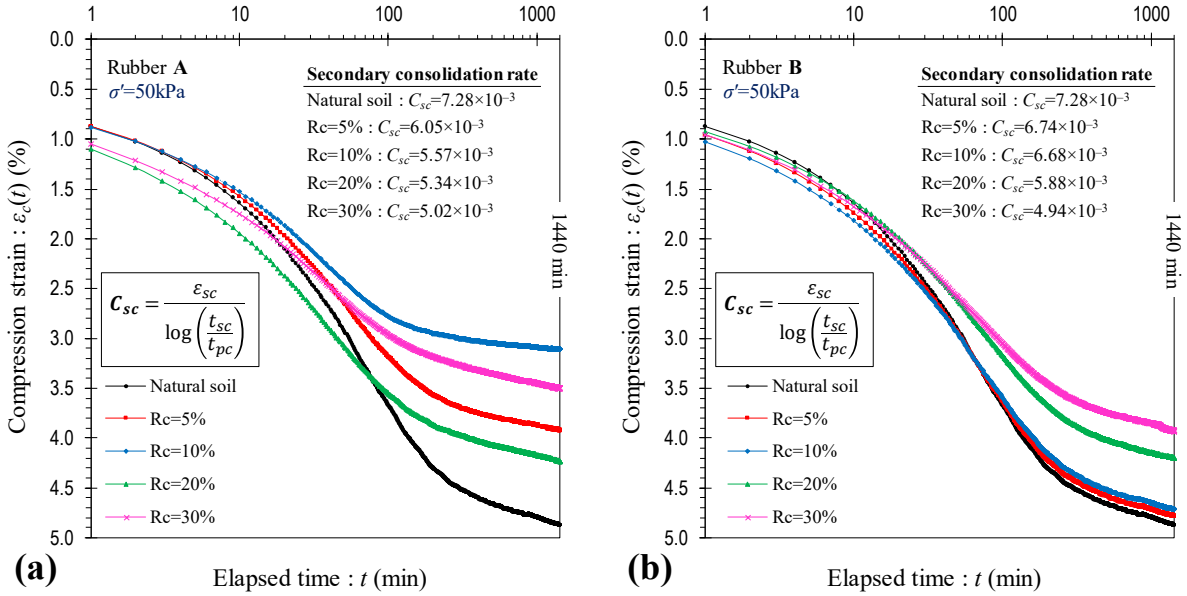

Figure 10. Secondary consolidation characteristics (under σ'=50 kPa) for the natural soil and various soil–rubber composites: **(a)** rubber A; and **(b)** rubber B.

3.3. *Effect of Rubbers on the Shrinkage Potential*

Void ratio–water content shrinkage curves, represented by the four–parameter logistic function (e.g. McGarry and Malafant 1987; Peng and Horn 2005; Thyagaraj et al. 2017), along with corresponding 100% saturation lines, for the natural soil and various soil–rubber composites are provided in **Figures 11a** and **11b** for rubbers A and B, respectively. Similar to the swell path, a typical shrink path (see path O→B_2 in **Figure 4c**) develops into an *S*–shaped curve, and thus can be divided into three regions, i.e. the structural, primary and residual shrinkage, which are defined as phases during which shrinkage takes place (Haines 1923; Tripathy et al. 2002; Cornelis et al. 2006; Estabragh et al. 2013b, 2015). In the structural shrinkage phase, the decrease in volume of the soil is less than the volume of water lost from the stable void spaces. This portion of the shrinkage curve constitutes for small volume changes, and is graphically represented by a mild–sloped curvilinear relationship. During primary shrinkage, also commonly referred to as normal shrinkage, the decrease in volume of the soil is essentially equal to the volume of lost water, thereby preventing the entrance of air into the soil pores. This portion of the shrinkage curve is represented by a steep–sloped linear relationship, which is theoretically parallel to the Sr=100% saturation line. The primary shrinkage phase extends up to the shrinkage limit, which marks a transitional state where the rate of volume change rapidly decreases, i.e. $\Delta e/\Delta\omega \rightarrow 0$. The majority of volume decrease takes place during the primary shrinkage phase. Completion of the primary shrinkage phase is further accompanied by residual shrinkage, where the entrance of air is allowed into the soil pores, thereby resulting in air–filled porosity. As a consequence of particles coming in contact, the decrease in volume of the soil becomes less than the volume of lost water. The magnitude of structural, primary and residual shrinkage strains, i.e. ε_{ssh}, ε_{psh} and ε_{rsh}, can be obtained by the following relationships (Mishra et al. 2008; Thyagaraj et al. 2017):

$$\varepsilon_{ssh} = \frac{\Delta e}{1+e_{ssw}}\Bigg]_{e_{ssh}}^{e_{ssw}} = \frac{e_{ssw}-e_{ssh}}{1+e_{ssw}} \tag{4}$$

$$\varepsilon_{psh} = \frac{\Delta e}{1+e_{ssh}}\Bigg]_{e_{psh}}^{e_{ssh}} = \frac{e_{ssh}-e_{psh}}{1+e_{ssh}} \quad (5)$$

$$\varepsilon_{rsh} = \frac{\Delta e}{1+e_{psh}}\Bigg]_{e_{rsh}}^{e_{psh}} = \frac{e_{psh}-e_{rsh}}{1+e_{psh}} \quad (6)$$

where as outlined in **Figure 4c**, e_{ssw}=void ratio at the swollen state A (i.e. the end of secondary swelling); e_{ssh}=void ratio at the end of structural shrinkage; e_{psh}=void ratio at the end of primary shrinkage (or at the shrinkage limit); and e_{rsh}=void ratio at the fully desiccated state B_2.

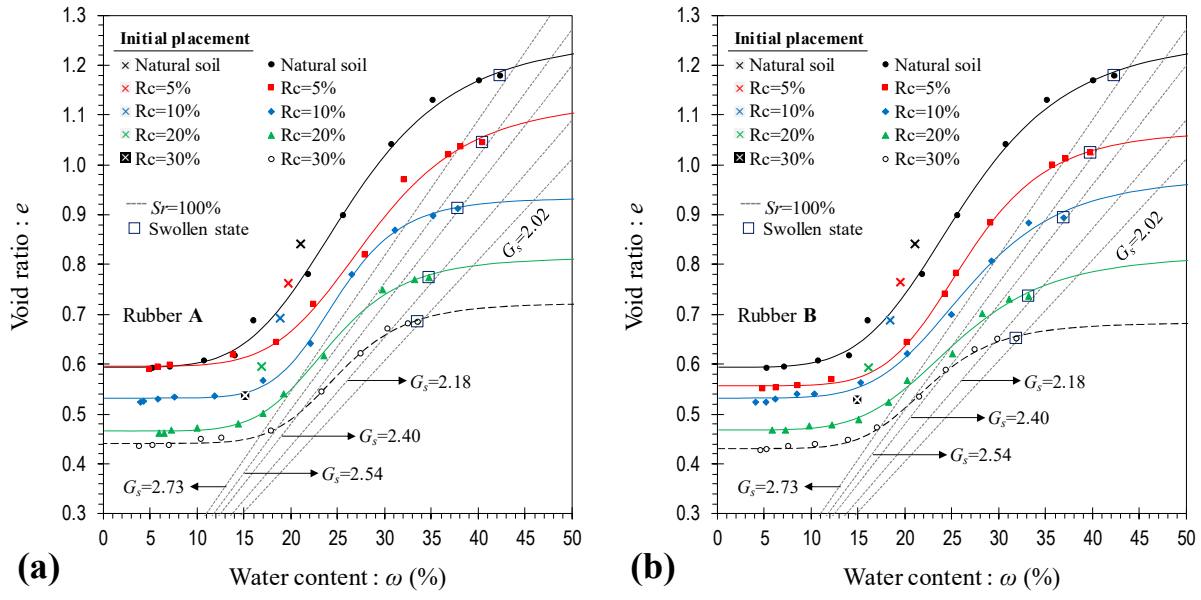

Figure 11. Void ratio–water content shrinkage curves for the natural soil and various soil–rubber composites: **(a)** rubber A; and **(b)** rubber B.

The total shrinkage strain, denoted as the shrinkage potential, can be defined as $SH_p=\varepsilon_{ssh}+\varepsilon_{psh}+\varepsilon_{rsh}$. The shrinkage strains and the shrinkage limit for the tested samples are presented in **Table 5**. The shrinkage strains demonstrated a rubber content–dependency, meaning that the greater the rubber content the lower the shrinkage strains. The effect of rubber size, however, was observed to be marginal for the majority of cases. The shrinkage potential demonstrated a trend similar to that observed for the swelling potential. The natural soil displayed a shrinkage potential of SH_p=28.60%. Soil–rubber A mixtures corresponding to R_c=5%, 10%, 20% and 30% resulted in SH_p=23.44%, 21.30%, 18.27% and 15.30%, respectively. Similar inclusions of rubber B promoted slightly lower values, and were measured as SH_p=24.61%, 20.44%, 16.01% and 14.04%, respectively. As a result of rubber–reinforcement, the shrinkage limit experienced a minor increase; however, the resulted variations were observed to be less dependent on rubber content and rubber size.

Table 5. Shrinkage strains and the shrinkage limit for the tested samples.

Sample	R_c (%)	ε_{ssh} (%)	ε_{psh} (%)	ε_{rsh} (%)	SH_p (%)	SL (%) [1]
–	–	4.15	21.47	2.98	28.60	14.88
Rubber A based sample	5	2.99	17.50	2.95	23.44	17.82
	10	3.07	15.53	2.71	21.30	18.00
	20	2.49	13.62	2.15	18.27	16.25
	30	2.01	11.24	2.06	15.30	17.86
Rubber B based sample	5	3.54	18.16	2.92	24.61	17.67
	10	2.43	15.33	2.68	20.44	16.40
	20	1.83	12.33	1.85	16.01	15.16
	30	1.86	10.43	1.75	14.04	15.18

[1] shrinkage limit.

3.4. *Effect of Rubbers on the Strength Properties*

Stress–strain curves, obtained from the unconfined compression tests, for the natural soil and various soil–rubber composites are provided in **Figures 12a** and **12b** for rubbers A and B, respectively. The natural soil displayed a peak strength of q_u=113 kPa, while the inclusion of 5% rubbers A and B resulted in q_u=129 kPa and 142 kPa, respectively. With R_c=10%, q_u dropped to 128 kPa (for rubber A) and 127 kPa (for rubber B), which still maintains a noticeable advantage over the natural soil. Higher rubber inclusions, i.e. 20% and 30%, however, gave rise to lower q_u values compared to that observed for the natural soil (i.e. q_u=102kPa and 98 kPa for 20% rubbers A and B; and q_u=72 kPa and 88 kPa for 30% rubbers A and B). It is noteworthy to cross check q_u with S_p, P_s and SH_p, which are in favor of a higher rubber content. This discrepancy implies that even though the rubbers are consistently effective at weaving the soil into a coherent matrix of restricted heave and settlement, when excessively included raise strength concerns.

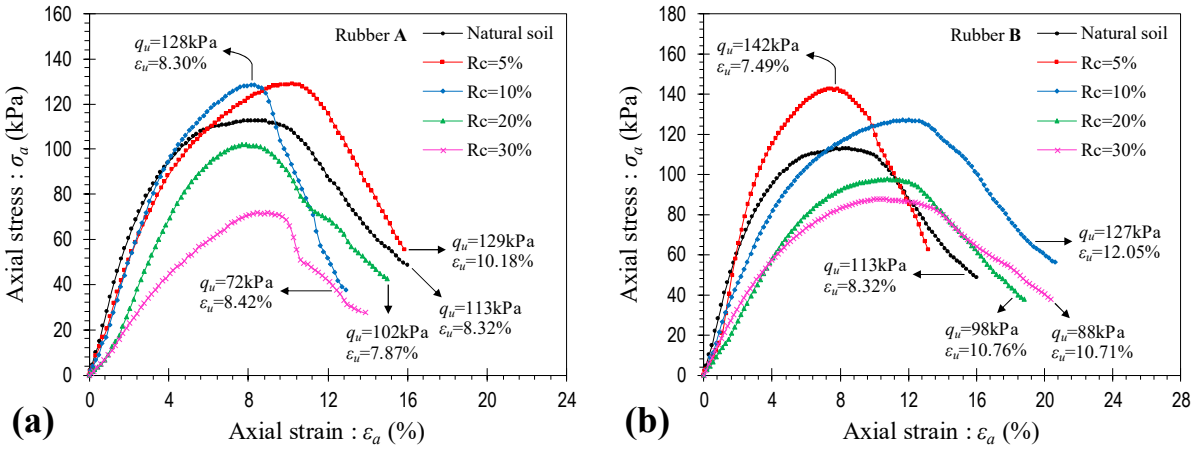

Figure 12. Stress–strain unconfined compression curves for the natural soil and various soil–rubber composites: **(a)** rubber A; and **(b)** rubber B.

Figure 13 illustrates the variations of strain energy at peak E_p along with corresponding q_u values against rubber content for the tested samples. The variations of E_p followed a trend quite similar to that observed for q_u. A noticeable improvement in the ductility can be achieved for rubber inclusions equal to or less than 10%, while the higher rubber inclusions of 20% and 30% gave rise to a less ductile character, and thus a rather brittle sample failure. Although in terms of q_u, the performance of both rubber types seemed to be on par with each other, soil–rubber B mixtures consistently (an exception was R_c=5%) promoted a higher ductility (i.e. higher E_p) compared to similar samples reinforced with rubber A. As optimum cases, E_p increased from 6.91 kJ/m^3 for the natural soil to 9.04 kJ/m^3 and 10.84 kJ/m^3 for the samples reinforced with 5% rubber A and 10% rubber B, respectively. The elastic stiffness modulus E_{50}, defined as the secant modulus at 50% of the peak strength (Radovic et al. 2004; Iyengar et al. 2013), was also measured for the tested samples. In general, the greater the rubber content the lower the E_{50} value, following a monotonic trend. Expect for 5% rubber B, all samples exhibited a lower E_{50} compared to the natural soil. The natural soil resulted in E_{50}=3.15 MPa, while the inclusion of 5%, 10%, 20% and 30% rubber A resulted in E_{50}=2.47 MPa, 2.56 MPa, 1.69 MPa and 1.15 MPa, respectively. Similar inclusions of rubber B did not significantly deviate the aforementioned values (an exception was R_c=5%), and resulted in E_{50}=3.27 MPa, 2.19 MPa, 1.45 MPa and 1.59 MPa, respectively.

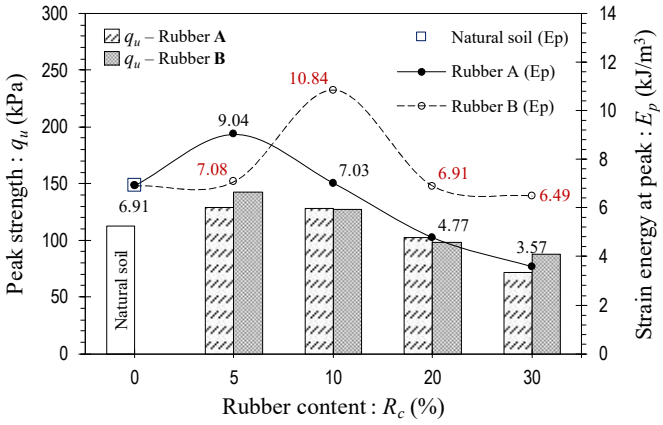

Figure 13. Variations of strain energy at peak and the peak strength against rubber content for the tested samples.

3.5. *Amending Mechanisms*

Similar to fiber–reinforced soils, the rubber inclusions are able to amend the soil fabric through improvements achieved in three aspects, i.e. increase in non–expansive fraction or non–wetting attribute (Viswanadham et al. 2009a; Patil et al. 2011; Trouzine et al. 2012; Estabragh et al. 2014; Soltani et al. 2017a), interlocking of rubber particles and soil grains (Tang et al. 2007, 2010; Kalkan 2013; Phanikumar and Singla 2016), and frictional resistive forces generated as a result of soil–rubber contact (Cai et al. 2006; Al-Akhras et al. 2008; Viswanadham et al. 2009b; Patil et al. 2011; Trouzine et al. 2012; Phanikumar and Singla 2016). The randomly distributed rubber particles resemble a spatial three–dimensional network in favor of weaving or interlocking the soil grains into a coherent matrix of restricted heave and settlement. The greater the number of included rubber particles, i.e. increase in rubber content, the more effective the interlocking effect. The frictional resistive forces grow as a consequence of rubber particles experiencing tensile/compressive stress in the presence of strong swelling/compression forces. Increase in rubber content leads to an increase in the total surface area, and thus a greater interfacial contact between rubber particles and soil grains. This in turn enhances the frictional effect between rubber particles, thereby mitigating the swell–shrink–consolidation capacity.

The swell–shrink–consolidation dependence on rubber size (or shape) is on par with the aspect ratio (i.e. fiber length to diameter ratio) in fiber–reinforced soils, and thus can be ascribed to the improvement mechanisms 'interlocking' and 'frictional resistive forces'. Increase in rubber size increases the soil–rubber contacts, which in turn generates a greater net frictional resistance between rubbers coupled with an enhanced soil–rubber interlocking effect. This improvement mechanism is also in line with rubber shape. As opposed to the granular form of rubber A, the particles of rubber B are relatively more fiber–shaped (see **Figure 2**); hence, they are more resilient to withstand (or translate) tensile/compressive stress along their axis, which in turn restricts the movement of soil particles interlocked to the rubber.

4. Optimum Rubber Content and Cost Analysis

The primary objective of any introduced stabilization scheme dealing with expansive soils should complement a decrease in the swell–shrink–consolidation capacity, while either maintaining or improving the strength–related properties (Soltani 2017). Although both rubber types are consistently effective at weaving the soil into a coherent matrix of restricted heave and settlement (i.e. improvement in the swell–shrink–consolidation capacity is in favor of higher rubber contents), excessive inclusions raise strength concerns. Based on the results presented in **Sections 3.1** to **3.4**, a maximum rubber inclusion of 10% seems to satisfy both objectives, and thus can be deemed as the optimum choice. Where context changes and the strength and stiffness is not a primary concern, higher rubber inclusions up to 20% may also be considered acceptable. The swell–shrink–consolidation properties were rubber size–dependent, meaning that the rubber of coarser size often outperformed the finer rubber. In terms of strength, however, the two rubber types promoted similar results with marginal differences. Therefore, the choice of rubber size would be dependent on design requirements and project objectives, rubber availability and costs.

Table 6 summarizes a comparative cost analysis performed for the reinforcement of an assumed mass of 1000 kg of soil using recycled tire rubbers and conventional poly– (ester, ethylene or propylene) and steel fibers. The unit price for both rubber types, poly and steel fibers were taken in accordance with common prices found in South Australian markets, which are approximately 0.5 AU$/kg, 14.3 AU$/kg and 2.2 AU$/kg, respectively. Other costs

such as transportation, labor and compaction have not been included as they are highly case– and region–dependent. Significant cost reduction can be achieved where rubbers are used as a replacement for conventional fibers. For instance, R_c=10% results in a total cost of 50 AU$, while the use of poly and steel fibers at their so–called optimum contents, i.e. f_c=0.8% and 10%, results in 114.4 AU$ and 220 AU$, respectively. Unlike fibers, the rubber–reinforcement technique requires a large quantity of rubber material to ameliorate the swell–shrink–consolidation capacity. However, in terms of total cost, it still maintains a significant advantage over conventional fibers. More importantly, beneficial reuse of recycled tires provides a sound environmental alternative to the safe disposal concern associated with such waste materials. The results of the cost analysis are in agreement with Yadav and Tiwari (2017), whom carried out a similar comparative analysis with respect to the Indian market.

Table 6. Comparative cost analysis between rubbers and conventional fibers.

Type of reinforcement	R_c (%)	f_c (%) [1]	Unit price (AU$/kg)	Total cost (AU$)
Rubber (A or B)	5	–	0.5	25.0
	10	–		50.0
	20	–		100.0
Poly– (ester, ethylene or propylene) fiber	–	0.8 [2]	14.3	114.4
Steel fiber	–	10 [3]	2.2	220

[1] fiber content (i.e. fiber to dry soil mass ratio); [2] suggested by Olgun (2013) and Shahbazi et al. (2017); and [3] suggested by Fatahi et al. (2012).

5. Conclusions

The following conclusions can be drawn from this study:

- As a result of rubber–reinforcement, the swelling strain–time locus experienced a major downward shift over the semi–log space, signifying a capacity to counteract the heave in both magnitude and time. Improvement in the rate and potential of swelling was dependent on both the rubber content and the rubber size, with the former taking on a more pronounced role. A similar dependency was also observed for the shrinkage potential. In this case, however, the effect of rubber size was observed to be marginal for the majority of cases.
- Rubber–reinforcement altered the void ratio–effective stress consolidation locus, resulting in a significant reduction in the swelling pressure. The variations of swelling pressure suggested a trend similar to that of swelling potential. In addition, the rubber inclusions led to a noticeable reduction in the compression and swell indices, indicating a capacity to counteract material collapse when stressed. The compression index was observed to be rubber size–dependent; however, for the swell index, the performance of both rubber types seemed to be on par with each other.
- The secondary consolidation rate also exhibited a rubber content/size–dependency, indicating a capacity to counteract the settlement in both magnitude and time. The greater the rubber content the lower the secondary consolidation rate, with the finer rubber maintaining a slight advantage over the coarser rubber. The resulted trends for the secondary swelling and secondary consolidation rates were observed to be consistent and comparable.
- The results of the unconfined compression tests were cross checked with the swell–shrink–consolidation properties to arrive the optimum stabilization scenarios. A maximum rubber inclusion of 10%, preferably the rubber of coarser category, proved to satisfy the stabilization objectives, and thus was deemed as the optimum choice. Where context changes and the strength and stiffness is not a primary concern, higher rubber inclusions up to 20% could also be considered acceptable.
- The cost efficiency of the rubber–reinforcement technique was compared to conventional poly– (ester, ethylene or propylene) and steel fibers. Significant cost reduction can be achieved where rubbers are used as a replacement for conventional fibers. More importantly, beneficial reuse of recycled tires provides a sound environmental alternative to the safe disposal concern associated with such waste materials.

Acknowledgements

This research was funded by the Australian Research Council (ARC) via project No. DP140103004, and their support is gratefully acknowledged.

References

Akbulut, S., Arasan, S., and Kalkan, E., 2007, "Modification of Clayey Soils Using Scrap Tire Rubber and Synthetic Fibers," *Appl. Clay Sci.*, Vol. 38, No. 1–2, pp. 23–32. doi:10.1016/J.CLAY.2007.02.001.

Al-Akhras, N. M., Attom, M. F., Al-Akhras, K. M., and Malkawi, A. I. H., 2008, "Influence of Fibers on Swelling Properties of Clayey Soil," *Geosynth. Int.*, Vol. 15, No. 4, pp. 304–309. doi:10.1680/GEIN.2008.15.4.304.

Alazigha, D. P., Indraratna, B., Vinod, J. S., and Ezeajugh, L. E., 2016, "The Swelling Behaviour of Lignosulfonate–Treated Expansive Soil," *Proc. ICE Gr. Improv.*, Vol. 169, No. 3, pp. 182–193. doi:10.1680/JGRIM.15.00002.

Al-Rawas, A. A., Hago, A. W., and Al-Sarmi, H., 2005, "Effect of Lime, Cement and Sarooj (Artificial Pozzolan) on the Swelling Potential of an Expansive Soil from Oman," *Build. Environ.*, Vol. 40, No. 5, pp. 681–687. doi:10.1016/J.BUILDENV.2004.08.028.

Ang, E. C., and Loehr, J. E., 2003, "Specimen Size Effects for Fiber–Reinforced Silty Clay in Unconfined Compression," *Geotech. Test. J.*, Vol. 26, No. 2, pp. 191–200. doi:10.1520/GTJ11320J.

AS 1289.3.2.1:09, 2009, *Methods of Testing Soils for Engineering Purposes: Soil Classification Tests–Determination of the Plastic Limit of a Soil*, Standards Australia, Sydney, NSW.

AS 1289.3.3.1:09, 2009, *Methods of Testing Soils for Engineering Purposes: Soil Classification Tests–Calculation of the Plasticity Index of a Soil*, Standards Australia, Sydney, NSW.

AS 1289.3.4.1:08, 2008, *Methods of Testing Soils for Engineering Purposes: Soil Classification Tests–Determination of the Linear Shrinkage of a Soil*, Standards Australia, Sydney, NSW.

AS 1289.3.9.1:15, 2015, *Methods of Testing Soils for Engineering Purposes: Soil Classification Tests–Determination of the Cone Liquid Limit of a Soil*, Standards Australia, Sydney, NSW.

ASTM D2166/D2166M-16, 2016, *Standard Test Method for Unconfined Compressive Strength of Cohesive Soil*, ASTM International, West Conshohocken, PA. doi:10.1520/D2166_D2166M-16.

ASTM D2487-11, 2011, *Standard Practice for Classification of Soils for Engineering Purposes (Unified Soil Classification System)*, ASTM International, West Conshohocken, PA. doi:10.1520/D2487-11.

ASTM D422-63(2007)e2, 2007, *Standard Test Method for Particle–Size Analysis of Soils*, ASTM International, West Conshohocken, PA. doi:10.1520/D0422-63R07E02.

ASTM D427-04, 2004, *Test Method for Shrinkage Factors of Soils by the Mercury Method*, ASTM International, West Conshohocken, PA. doi:10.1520/D0427-04.

ASTM D4546-14, 2014, *Standard Test Methods for One–Dimensional Swell or Collapse of Soils*, ASTM International, West Conshohocken, PA. doi:10.1520/D4546.

ASTM D698-12e2, 2012, *Standard Test Methods for Laboratory Compaction Characteristics of Soil Using Standard Effort (12,400 ft–lbf/ft³ (600 kN–m/m³))*, ASTM International, West Conshohocken, PA. doi:10.1520/D0698-12E02.

ASTM D854-14, 2014, *Standard Test Methods for Specific Gravity of Soil Solids by Water Pycnometer*, ASTM International, West Conshohocken, PA. doi:10.1520/D0854-14.

Cai, Y., Shi, B., Ng, C. W. W., and Tang, C. S., 2006, "Effect of Polypropylene Fibre and Lime Admixture on Engineering Properties of Clayey Soil," *Eng. Geol.*, Vol. 87, No. 3–4, pp. 230–240. doi:10.1016/J.ENGGEO.2006.07.007.

Casagrande, A., 1936, "The Determination of Pre–Consolidation Load and Its Practical Significance," In: Casagrande, A., Rutledge, P. C., and Watson, J. D. (Eds.), *First International Conference on Soil Mechanics and Foundation Engineering*, ASCE, Cambridge, MA, pp. 60–64.

Cetin, H., Fener, M., and Gunaydin, O., 2006, "Geotechnical Properties of Tire–Cohesive Clayey Soil Mixtures as a Fill Material," *Eng. Geol.*, Vol. 88, No. 1–2, pp. 110–120. doi:10.1016/J.ENGGEO.2006.09.002.

Cornelis, W. M., Corluy, J., Medina, H., Díaz, J., Hartmann, R., van Meirvenne, M., and Ruiz, M. E., 2006, "Measuring and Modelling the Soil Shrinkage Characteristic Curve," *Geoderma*, Vol. 137, No. 1–2, pp. 179–191. doi:10.1016/J.GEODERMA.2006.08.022.

Dakshanamurthy, V., 1978, "A New Method to Predict Swelling Using Hyperbola Equation," *Geotech. Eng. J. SEAGS AGSSEA*, Vol. 8, No. 1, pp. 29–38.

Dif, A., and Bluemel, W., 1991, "Expansive Soils under Cyclic Drying and Wetting," *Geotech. Test. J.*, Vol. 14, No. 1, pp. 96–102. doi:10.1520/GTJ10196J.

Dunham-Friel, J., and Carraro, J. A. H., 2011, "Shear Strength and Stiffness of Expansive Soil and Rubber (ESR) Mixtures in Undrained Axisymmetric Compression," In: Han, J., and Alzamora, D. E. (Eds.), *Geo–Frontiers 2011: Advances in Geotechnical Engineering (GSP 211)*, ASCE, Dallas, TX, pp. 1111–1120. doi:10.1061/41165(397)114.

Edil, T., and Bosscher, P., 1994, "Engineering Properties of Tire Chips and Soil Mixtures," *Geotech. Test. J.*, Vol. 17, No. 4, pp. 453–464. doi:10.1520/GTJ10306J.

Estabragh, A. R., Moghadas, M., and Javadi, A. A., 2013b, "Effect of Different Types of Wetting Fluids on the Behaviour of Expansive Soil during Wetting and Drying," *Soils Found.*, Vol. 53, No. 5, pp. 617–627. doi:10.1016/J.SANDF.2013.08.001.

Estabragh, A. R., Parsaei, B., and Javadi, A. A., 2015, "Laboratory Investigation of the Effect of Cyclic Wetting and Drying on the Behaviour of an Expansive Soil," *Soils Found.*, Vol. 55, No. 2, pp. 304–314. doi:10.1016/J.SANDF.2015.02.007.

Estabragh, A. R., Pereshkafti, M. R. S., Parsaei, B., and Javadi, A. A., 2013a, "Stabilised Expansive Soil Behaviour during Wetting and Drying," *Int. J. Pavement Eng.*, Vol. 14, No. 4, pp. 418–427. doi:10.1080/10298436.2012.746688.

Estabragh, A. R., Rafatjo, H., and Javadi, A. A., 2014, "Treatment of an Expansive Soil by Mechanical and Chemical Techniques," *Geosynth. Int.*, Vol. 21, No. 3, pp. 233–243. doi:10.1680/GEIN.14.00011.

Fatahi, B., Khabbaz, H., and Fatahi, B., 2012, "Mechanical Characteristics of Soft Clay Treated with Fibre and Cement," *Geosynth. Int.*, Vol. 19, No. 3, pp. 252–262. doi:10.1680/GEIN.12.00012.

Haines, W. B., 1923, "The Volume–Changes Associated with Variations of Water Content in Soil," *J. Agric. Sci.*, Vol. 13, No. 3, pp. 296–310. doi:10.1017/S0021859600003580.

Hanafy, E. A. D. E., 1991, "Swelling/Shrinkage Characteristic Curve of Desiccated Expansive Clays," *Geotech. Test. J.*, Vol. 14, No. 2, pp. 206–211. doi:10.1520/GTJ10562J.

Hannam, P., 2014, "Tyre Industry Divided over How to Handle Toxic Waste," *The Sydney Morning Herald*, Sydney, NSW, http://www.smh.com.au/environment/tyre-industry-divided-over-how-to-handle-toxic-waste-20140120-314ic.html. (accessed 8/10/2017)

Iyengar, S. R., Masad, E., Rodriguez, A. K., Bazzi, H. S., Little, D., and Hanley, H. J. M., 2013, "Pavement Subgrade Stabilization Using Polymers: Characterization and Performance," *J. Mater. Civ. Eng.*, Vol. 25, No. 4, pp. 472–483. doi:10.1061/(ASCE)MT.1943-5533.0000612.

Jha, A. K., and Sivapullaiah, P. V., 2016, "Gypsum–Induced Volume Change Behavior of Stabilized Expansive Soil With Fly Ash–Lime," *Geotech. Test. J.*, Vol. 39, No. 3, pp. 391–406. doi:10.1520/GTJ20150017.

Jones, L. D., and Jefferson, I., 2012, "Expansive Soils," In: Burland, J., Chapman, T., Brown, M., and Skinner, H. (Eds.), *ICE Manual of Geotechnical Engineering: Volume I*, ICE Publishing, London, pp. 413–441. doi:10.1680/MOGE.57074.0413.

Jose, B. T., Sridharan, A., and Abraham, B. M., 1989, "Log–Log Method for Determination of Preconsolidation Pressure," *Geotech. Test. J.*, Vol. 12, No. 3, pp. 230–237. doi:10.1520/GTJ10974J.

Kalkan, E., 2013, "Preparation of Scrap Tire Rubber Fiber–Silica Fume Mixtures for Modification of Clayey Soils," *Appl. Clay Sci.*, Vol. 80–81, pp. 117–125. doi:10.1016/J.CLAY.2013.06.014.

Maher, M. H., and Ho, Y. C., 1994, "Mechanical Properties of Kaolinite/Fiber Soil Composite," *J. Geotech. Eng.*, Vol. 120, No. 8, pp. 1381–1393. doi:10.1061/(ASCE)0733-9410(1994)120:8(1381).

McGarry, D., and Malafant, K. W. J., 1987, "The Analysis of Volume Change in Unconfined Units of Soil," *Soil Sci. Soc. Am. J.*, Vol. 51, No. 2, pp. 290–297. doi:10.2136/SSSAJ1987.03615995005100020059X.

Mirzababaei, M., Miraftab, M., Mohamed, M., and McMahon, P., 2013a, "Impact of Carpet Waste Fibre Addition on Swelling Properties of Compacted Clays," *Geotech. Geol. Eng.*, Vol. 31, No. 1, pp. 173–182. doi:10.1007/S10706-012-9578-2.

Mirzababaei, M., Miraftab, M., Mohamed, M., and McMahon, P., 2013b, "Unconfined Compression Strength of Reinforced Clays with Carpet Waste Fibers," *J. Geotech. Geoenvironmental Eng.*, Vol. 139, No. 3, pp. 483–493. doi:10.1061/(ASCE)GT.1943-5606.0000792.

Mirzababaei, M., Yasrobi, S. S., and Al-Rawas, A. A., 2009, "Effect of Polymers on Swelling Potential of Expansive Soils," *Proc. ICE Gr. Improv.*, Vol. 162, No. 3, pp. 111–119. doi:10.1680/GRIM.2009.162.3.111.

Mishra, A. K., Dhawan, S., and Rao, S. M., 2008, "Analysis of Swelling and Shrinkage Behavior of Compacted Clays," *Geotech. Geol. Eng.*, Vol. 26, No. 3, pp. 289–298. doi:10.1007/S10706-007-9165-0.

Nalbantoglu, Z., 2006, "Lime Stabilization of Expansive Clay," In: Al-Rawas, A. A., and Goosen, M. F. A. (Eds.), *Expansive soils: Recent Advances in Characterization and Treatment*, Taylor & Francis Group, London, pp. 139–148. doi:10.1201/9780203968079.CH23.

Olgun, M., 2013, "The Effects and Optimization of Additives for Expansive Clays under Freeze–Thaw Conditions," *Cold Reg. Sci. Technol.*, Vol. 93, pp. 36–46. doi:10.1016/J.COLDREGIONS.2013.06.001.

Onyejekwe, S., and Ghataora, G. S., 2015, "Soil Stabilization Using Proprietary Liquid Chemical Stabilizers: Sulphonated Oil and a Polymer," *Bull. Eng. Geol. Environ.*, Vol. 74, No. 2, pp. 651–665. doi:10.1007/S10064-014-0667-8.

Özkul, Z., and Baykal, G., 2007, "Shear Behavior of Compacted Rubber Fiber–Clay Composite in Drained and Undrained Loading," *J. Geotech. Geoenvironmental Eng.*, Vol. 133, No. 7, pp. 767–781. doi:10.1061/(ASCE)1090-0241(2007)133:7(767).

Pacheco Silva, F., 1970, "A New Graphical Construction for Determination of the Preconsolidation Stress of a Soil Sample," In: *Proceedings of the Fourth Brazilian Conference on Soil Mechanics and Foundation Engineering*, Rio de Janeiro, pp. 225–232.

Patil, U., Valdes, J. R., and Evans, T. M., 2011, "Swell Mitigation with Granulated Tire Rubber," *J. Mater. Civ. Eng.*, Vol. 23, No. 5, pp. 721–727. doi:10.1061/(ASCE)MT.1943-5533.0000229.

Peng, X., and Horn, R., 2005, "Modeling Soil Shrinkage Curve across a Wide Range of Soil Types," *Soil Sci. Soc. Am. J.*, Vol. 69, No. 3, pp. 584–592. doi:10.2136/SSSAJ2004.0146.

Phanikumar, B. R., and Singla, R., 2016, "Swell–Consolidation Characteristics of Fibre–Reinforced Expansive Soils," *Soils Found.*, Vol. 56, No. 1, pp. 138–143. doi:10.1016/J.SANDF.2016.01.011.

Prakash, K., and Sridharan, A., 2004, "Free Swell Ratio and Clay Mineralogy of Fine–Grained Soils," *Geotech. Test. J.*, Vol. 27, No. 2, pp. 220–225. doi:10.1520/GTJ10860.

Radovic, M., Lara-Curzio, E., and Riester, L., 2004, "Comparison of Different Experimental Techniques for Determination of Elastic Properties of Solids," *Mater. Sci. Eng. A*, Vol. 368, No. 1–2, pp. 56–70. doi:10.1016/J.MSEA.2003.09.080.

Rao, S. M., Thyagaraj, T., and Thomas, H. R., 2006, "Swelling of Compacted Clay under Osmotic Gradients," *Géotechnique*, Vol. 56, No. 10, pp. 707–713. doi:10.1680/GEOT.2006.56.10.707.

Seda, J. H., Lee, J. C., and Carraro, J. A. H., 2007, "Beneficial Use of Waste Tire Rubber for Swelling Potential Mitigation in Expansive Soils," In: Schaefer, V. R., Filz, G. M., Gallagher, P. M., Sehn, A. L., and Wissmann, K. J. (Eds.), *Geo–Denver 2007: Soil Improvement (GSP 172)*, ASCE, Denver, CO, pp. 1–9. doi:10.1061/40916(235)5.

Shahbazi, M., Rowshanzamir, M., Abtahi, S. M., and Hejazi, S. M., 2017, "Optimization of Carpet Waste Fibers and Steel Slag Particles to Reinforce Expansive Soil Using Response Surface Methodology," *Appl. Clay Sci.*, Vol. 142, No. 15, pp. 185–192. doi:10.1016/J.CLAY.2016.11.027.

Sibley, J. W., and Williams, D. J., 1989, "A Procedure for Determining Volumetric Shrinkage of an Unsaturated Soil," *Geotech. Test. J.*, Vol. 12, No. 3, pp. 181–187. doi:10.1520/GTJ10966J.

Signes, C. H., Garzón-Roca, J., Fernández, P. M., Torre, M. E. G., and Franco, R. I., 2016, "Swelling Potential Reduction of Spanish Argillaceous Marlstone Facies Tap Soil through the Addition of Crumb Rubber Particles from Scrap Tyres," *Appl. Clay Sci.*, Vol. 132–133, pp. 768–773. doi:10.1016/J.CLAY.2016.07.027.

Sivapullaiah, P. V., Sridharan, A., and Stalin, V. K., 1996, "Swelling Behaviour of Soil–Bentonite Mixtures," *Can. Geotech. J.*, Vol. 33, No. 5, pp. 808–814. doi:10.1139/T96-106-326.

Soltani, A., 2017, "Discussion of 'Optimization of Carpet Waste Fibers and Steel Slag Particles to Reinforce Expansive Soil Using Response Surface Methodology' by M. Shahbazi, M. Rowshanzamir, S.M. Abtahi, S.M. Hejazi [Appl. Clay Sci., doi:10.1016/j.clay.2016.11.027]," *Appl. Clay Sci.*, in press. doi:10.1016/J.CLAY.2017.07.020.

Soltani, A., Deng, A., Taheri, A., Sridharan, A., and Estabragh, A. R., 2017b, "A Framework for Interpretation of the Compressibility Behavior of Soils," *Geotech. Test. J.*, in press.

Soltani, A., Taheri, A., Khatibi, M., and Estabragh, A. R., 2017a, "Swelling Potential of a Stabilized Expansive Soil: A Comparative Experimental Study," *Geotech. Geol. Eng.*, Vol. 35, No. 4, pp. 1717–1744. doi:10.1007/S10706-017-0204-1.

Sridharan, A., Abraham, B. M., and Jose, B. T., 1991, "Improved Technique for Estimation of Preconsolidation Pressure," *Géotechnique*, Vol. 41, No. 2, pp. 263–268. doi:10.1680/GEOT.1991.41.2.263.

Sridharan, A., and Gurtug, Y., 2004, "Swelling Behaviour of Compacted Fine–Grained Soils," *Eng. Geol.*, Vol. 72, No. 1, pp. 9–18. doi:10.1016/S0013-7952(03)00161-3.

Sridharan, A., Rao, A., and Sivapullaiah, P., 1986, "Swelling Pressure of Clays," *Geotech. Test. J.*, Vol. 9, No. 1, pp. 24–33. doi:10.1520/GTJ10608J.

Srivastava, A., Pandey, S., and Rana, J., 2014, "Use of Shredded Tyre Waste in Improving the Geotechnical Properties of Expansive Black Cotton Soil," *Geomech. Geoengin.*, Vol. 9, No. 4, pp. 303–311. doi:10.1080/17486025.2014.902121.

Subba Rao, K. S., Rao, S. M., and Gangadhara, S., 2000, "Swelling Behavior of a Desiccated Clay," *Geotech. Test. J.*, Vol. 23, No. 2, pp. 193–198. doi:10.1520/GTJ11043J.

Tang, C. S., Shi, B., and Zhao, L. Z., 2010, "Interfacial Shear Strength of Fiber Reinforced Soil," *Geotext. Geomembranes*, Vol. 28, No. 1, pp. 54–62. doi:10.1016/J.GEOTEXMEM.2009.10.001.

Tang, C. S., Shi, B., Gao, W., Chen, F., and Cai, Y., 2007, "Strength and Mechanical Behavior of Short Polypropylene Fiber Reinforced and Cement Stabilized Clayey Soil," *Geotext. Geomembranes*, Vol. 25, No. 3, pp. 194–202. doi:10.1016/J.GEOTEXMEM.2006.11.002.

Thyagaraj, T., and Zodinsanga, S., 2014, "Swell–Shrink Behaviour of Lime Precipitation Treated Soil," *Proc. ICE Gr. Improv.*, Vol. 167, No. 4, pp. 260–273. doi:10.1680/GRIM.12.00028.

Thyagaraj, T., Thomas, S. R., and Das, A. P., 2017, "Physico–Chemical Effects on Shrinkage Behavior of Compacted Expansive Clay," *Int. J. Geomech.*, Vol. 17, No. 2, pp. 06016013-1–06016013-11. doi:10.1061/(ASCE)GM.1943-5622.0000698.

Tripathy, S., and Subba Rao, K. S., 2009, "Cyclic Swell–Shrink Behaviour of a Compacted Expansive Soil," *Geotech. Geol. Eng.*, Vol. 27, No. 1, pp. 89–103. doi:10.1007/S10706-008-9214-3.

Tripathy, S., Subba Rao, K. S., and Fredlund, D. G., 2002, "Water Content–Void Ratio Swell–Shrink Paths of Compacted Expansive Soils," *Can. Geotech. J.*, Vol. 39, No. 4, pp. 938–959. doi:10.1139/T02-022.

Trouzine, H., Bekhiti, M., and Asroun, A., 2012, "Effects of Scrap Tyre Rubber Fibre on Swelling Behaviour of Two Clayey Soils in Algeria," *Geosynth. Int.*, Vol. 19, No. 2, pp. 124–132. doi:10.1680/GEIN.2012.19.2.124.

Viswanadham, B. V. S., Phanikumar, B. R., and Mukherjee, R. V., 2009b, "Effect of Polypropylene Tape Fibre Reinforcement on Swelling Behaviour of an Expansive Soil," *Geosynth. Int.*, Vol. 16, No. 5, pp. 393–401. doi:10.1680/GEIN.2009.16.5.393.

Viswanadham, B. V. S., Phanikumar, B. R., and Mukherjee, R. V., 2009a, "Swelling Behaviour of a Geofiber–Reinforced Expansive Soil," *Geotext. Geomembranes*, Vol. 27, No. 1, pp. 73–76. doi:10.1016/J.GEOTEXMEM.2008.06.002.

Winterkorn, H. F., and Pamukcu, S., 1991, "Soil Stabilization and Grouting," In: Fang, H. Y. (Ed.), *Foundation Engineering Handbook*, Springer, New York, NY, pp. 317–378. doi:10.1007/978-1-4615-3928-5_9.

Yadav, J. S., and Tiwari, S. K., 2017, "A Study on the Potential Utilization of Crumb Rubber in Cement Treated Soft Clay," *J. Build. Eng.*, Vol. 9, pp. 177–191. doi:10.1016/J.JOBE.2017.01.001.

Zornberg, J. G., Cabral, A. R., and Viratjandr, C., 2004, "Behaviour of Tire Shred–Sand Mixtures," *Can. Geotech. J.*, Vol. 41, No. 2, pp. 227–241. doi:10.1139/T03-086.